Summer Student 2023
September 18, 2023

Feasibility Investigation into Detecting $D_s^+ \to \tau^+ + \nu_\tau$ in pNe Collisions at LHCb

Sungsoo Kim (Seoul National University)

Supervisors:
Jinlin Fu (University of Chinese Academy of Sciences, Beijing, China),
Chen Chen (Aix Marseille Univ, CNRS/IN2P3, CPPM, Marseille, France),
Mengzhen Wang (INFN Sezione di Milano, Milano, Italy)

Special thanks to **Nicola Neri** & **Andrea Merli** for their important contributions.

Abstract

In the pursuit of unraveling deeper insights into particle physics, this study delves into the feasibility of detecting the decay $D_s^+ \to \tau^+\nu_\tau$ in pNe collisions at LHCb. The primary focus lies on the $D_s^+ \to \tau^+\nu_\tau$ decay within the SMOG configuration, a pivotal stepping stone for the groundbreaking 'Bent Crystal' experiment. This decay holds profound implications for the Standard Model (SM) and the potential unveiling of New Physics (NP) phenomena. The study underscores the significance of suppressing the dominant charm background by employing Multivariate Analysis (MVA).

Targeting a signal-to-background ratio conducive to precise branch fraction determination, a Boosted Decision Tree (BDT) cut is set at $BDT > 5.65 \times 10^{-2}$. This BDT cut aims to enhance the discriminatory power of variables and facilitate Multivariable Fitting, enabling the extraction of the desired decay's branch fraction with reduced uncertainties.

For the purpose of observing the decay with a 5σ level of significance within the SMOG setup, an estimated integrated luminosity of $6.74\,\mathrm{pb}^{-1}$ is identified. This estimation surpasses the accumulated integrated luminosity of $200\,\mathrm{nb}^{-1}$ from the 2017 SMOG data, emphasizing the need for additional data to discern the desired decay from the background.

The research also underscores the potential of the 'Bent Crystal' experiment in measuring the Electric Dipole Moment (EDM) and Magnetic Dipole Moment (MDM) of the τ lepton. These measurements could serve as pivotal tools in probing the existence of New Physics. Future directions encompass generating ample Monte Carlo (MC) samples for multivariable fitting and exploring practical applications of bent crystals. This study serves as a foundational stride in bridging the gap between theoretical predictions and experimental measurements, offering a unique perspective to scrutinize the intricate landscape of particle physics.

Contents

1 Introduction

The primary objective of this project is to detect the decay $D_s^+ \to \tau^+\nu_\tau$ within the SMOG configuration. The project's motivation is twofold, encompassing both its potential to shed light on New Physics (NP) and its role as a stepping stone for the innovative 'Bent Crystal' experiment.

1.1 Potential Implications of $D_s^+ \to \tau^+\nu_\tau$ Decay

In the realm of the Standard Model (SM) of particle physics, the decay $D_s^+ \to \ell^+\nu_\ell$ holds crucial insights (1; 2; 3). For leptons ($\ell = e, \mu, \tau$), the branching fraction $B(D_s^+ \to \ell^+\nu_\ell)$ is characterized by Equation 1,

$$B\left(D_s^+ \to \ell^+\nu_\ell\right) = \frac{\tau_{D_s^+} m_{D_s^+}}{8\pi} f_{D_s^+}^2 G_F^2 \left|V_{cs}\right|^2 m_\ell^2 \left(1 - \frac{m_\ell^2}{m_{D_s^+}^2}\right)^2. \tag{1}$$

where the mass of the D_s^+ meson is denoted as m_{D_s}. Its lifetime is symbolized as τ_{D_s}. The term m_ℓ stands for the mass of the lepton. The pertinent CKM matrix component is represented by V_{cs}. Fermi's interaction is characterized by the constant G_F. The decay constant of the D_s^+ meson is given as f_{D_s}.

An important ratio emerges as $R_{\tau/\mu}^{D_s^+}$, connecting τ and μ decays, as described in Equation 2,

$$R_{\tau/\mu}^{D_s^+} \equiv \frac{B\left(D_s^{++} \to \tau^+\nu_\tau\right)}{B\left(D_s^{++} \to \mu^+\nu_\mu\right)} = \left(\frac{m_\tau}{m_\mu} \cdot \frac{1 - m_\tau^2/m_{D_s^+}^2}{1 - m_\mu^2/m_{D_s^+}^2}\right)^2. \tag{2}$$

This ratio $R_{\tau/\mu}^{D_s^+}$ is linked to Lepton Flavor Universality Violation (LFUV) within the SM. Furthermore, the value of $f_{D_s^+}|V_{cs}|$ can be determined from the branch fraction, and $f_{D_s^+}$ itself can be calculated through Lattice Quantum Chromodynamics (LQCD), connecting it with $|V_{cs}|$. Comparing these values can probe the accuracy of SM and LQCD predictions and unveil potential NP effects.

1.1.1 Experimental and Theoretical Comparison

Comparing experimental measurements and theoretical predictions, as summarized in Table 1, reveals slight deviations within the error range. Although these values overlap, achieving more precise measurements is imperative to narrow down uncertainties.

Table 1: Comparison of Experimental and Theoretical Values (1; 2; 3)

	$R_{\tau/\mu}^{D_s^+}$	$f_{D_s^+}$ (MeV)	$\|V_{cs}\|$
Experimental Measurement	9.89 ± 0.71	251.6 ± 10.8	0.97320 ± 0.00011
Theoretical Prediction (SM)	9.75 ± 0.01	248.0 ± 2.5	0.980 ± 0.042

1.2 Bent Crystal Experiment

The 'Bent Crystal' experiment holds considerable significance as a means to improve our understanding of particle decays(4). This method allows the measurement of the Electric Dipole Moment (EDM) and Magnetic Dipole Moment (MDM) of the τ lepton through the rotation of its spin. By comparing these measurements to theoretical calculations derived from the SM, we can evaluate the g factor of τ and potentially discern the presence of NP. The success of this method relies on the utilization of largely boosted τ particles, making fixed-target collisions essential.

This is where the System for Measuring Overlap with Gas (SMOG) configuration comes into play. While LHCb typically deals with pp collisions, the utilization of SMOG enables pNe collisions, which have a fixed-target feature. This is crucial for the 'Bent Crystal' experiment as it requires rapidly boosted τ particles. By studying the $D_s^+ \to \tau^+\nu_\tau$ decay in the SMOG configuration, we lay the groundwork for future 'Bent Crystal' experiments.

In summary, this project holds promise in not only detecting the $D_s^+ \to \tau^+\nu_\tau$ decay within the SMOG setup but also exploring its potential to reveal NP and to pave the way for transformative experiments like the 'Bent Crystal' technique. The intricate interplay between theoretical predictions and experimental measurements offers a unique opportunity to uncover fundamental aspects of particle physics.

2 Detector

The LHCb detector (5; 6) is a forward spectrometer uniquely designed to explore particles containing c or b quarks. It covers the pseudorapidity range $2 < \eta < 5$ in the lab frame. Key elements for this analysis include: the silicon-strip vertex locator (VELO), identifying c and b hadrons by their characteristic flight distances; a tracking system measuring charged particle momenta; two ring-imaging Cherenkov detectors, differentiating charged hadron species; a calorimeter with scintillating-pad and preshower detectors, electromagnetic and hadronic calorimeters; and a muon detector comprising iron and multiwire proportional chambers. The gas overlap measurement system (SMOG) (7) permits injecting gases with $\mathcal{O}(10^{-7})$ mbar pressure into the beam pipe section within VELO, enabling LHCb's operation as a fixed-target experiment. SMOG facilitates noble gas injection, uniquely enabling studies of nucleus-nucleus and proton-nucleus collisions for varied gaseous targets. Due to the boost from the high-energy proton beam in the positive-z direction, the LHCb acceptance encompasses the negative rapidity hemisphere in the center-of-mass system: $y^* \in [-2.29, 0]$.

3 Signal and Background

3.1 Motivation: Charm Background

The focus of our study lies in the observation of the signal process through the reconstruction of the 3π system:

$$D_s^+ \to \tau^+\nu_\tau \text{ with } \tau^+ \to 3\pi X,$$

where $3\pi \equiv \pi^+\pi^-\pi^+$ and X indicates the particles that could be created after the decay process.

However, the presence of charm background poses a significant challenge. This charm background comprises four possible inclusive decays, each occurring at a rate approximately

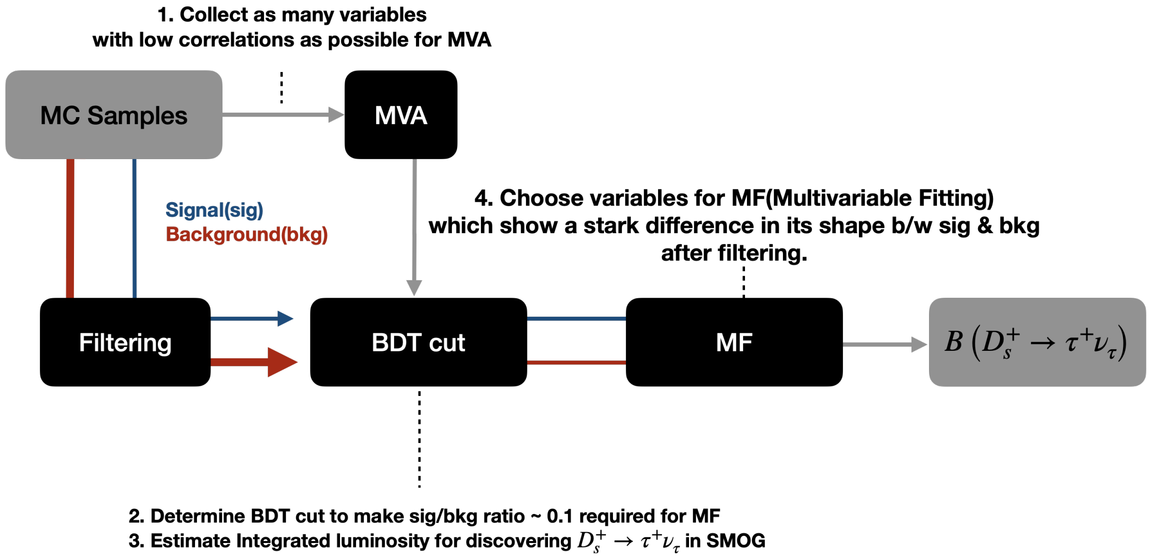

Figure 1: Roadmap outlining the steps of the entire process

more than 50 times larger than that of the signal process:

$$\begin{aligned} &D_s^+ \to 3\pi X\,, \\ &D^0 \to 3\pi X\,, \\ &D^+ \to 3\pi X\,, \\ &\Lambda_c^+ \to 3\pi X\,. \end{aligned}$$

Here, X represents the particles that might be produced through various inclusive decay processes, such as those involving τ. It's important to distinguish that the X in this context is different from the X in $\tau \to 3\pi X$. The key difference is in the origin of the decays: while the latter X originates from a direct decay, the former emerges from multiple inclusive decays.

Our primary objective is to effectively suppress these large charm backgrounds. By doing so, we aim to enhance our ability to observe the desired signal decay.

3.2 Goal and Road Map

The overarching goal of this study is to investigate the feasibility of detecting the signal process using Monte Carlo (MC) simulation samples. To achieve this, we outline a systematic approach that involves the suppression of the dominant charm background through the implementation of Multivariate Analysis (MVA) techniques. The road map for our investigation is as follows:

- Investigate the signal detection feasibility using MC samples.
- Employ MVA techniques to effectively suppress the large charm background
- Suppress background enough to perform MF to measure the branch fraction of the decay.
- Estimate the integrated luminosity for detection of the signal decay of 5σ.

The overall roadmap is illustrated in Fig. 1.

Table 2: Summary of combined samples with weights calculated using $w = \frac{fB}{N}$ where $\sigma \sim f$.(9; 10; 11; 13)

Dataset	Inclusive Decays	f (Fragmentation Function)	B	N (# of Generated Decays)
Signal.root	$Ds^+ \to \tau^+\nu_\tau \to 3\pi X$	0.0802	0.053	5125026
Ds_bkg.root	$Ds^+ \to 3\pi X$	0.0802	0.275	5016320
Dp_bkg.root	$D^- \to 3\pi X$	0.2404	0.146	5308008
Dz_bkg.root	$D^0 \to 3\pi X$	0.6086	0.161	5343095
Lc_bkg.root	$\Lambda_c^+ \to 3\pi X$	0.0623	0.246	3125313

3.3 Signal/Background Ratio Estimation

MC samples are produced for the signal and charm background decays to model the kinematic and topological distributions, as well as detector effects. The numbers of the MC events are aligned to be proportional to the expected fractions according to the production cross section and branching fractions, as shown in Table 2. This results in 553 signal events and 25,454 background events that can be used for analysis. The estimated sig/bkg ratio is 2.17×10^{-2}. This significant disparity of 50 times between the charm background and the signal underscores the need for strong background suppression strategies.

It's crucial to note that the signal and the four backgrounds are aggregated using weights obtained from normalizing the values presented in Table 2. After this weighted summation, the total count of the signal plus background post-filtering closely matches the size of one of the datasets (either signal or background) prior to the combination. Thus, while the size of original signal data after filtering is nearly 30,000 and not 553, the weight of the signal data, which is markedly lower than others, results in a surprisingly low size when merged with the background data.

3.4 Simulation and Data Cut

The configuration of charm meson decays is accomplished using the DecFiles within EvtGen. The simulations were executed using Davinci. The specific selection criteria are outlined below:

```
tau_3p1_cut = '(P > 3.0 GeV) & (PT > 250. * MeV) & (BPVIPCHI2 () > 4.8)
 & (TRCHI2DOF < 5) & (TRGHOSTPROB < 0.4) & (PIDK < 20)
MakeTau.DaughtersCuts = "pi+* tau_3p1_cut, : tau_3p1_cut,
MakeTau.CombinationCut = "((AM > 400. MeV) & (AM < 2060. MeV))
& (ADOCAMAX(**) < 0.15 mm) & ((AM12 < 1679. MeV) or (AH23 < 1678. MeV))
& (ANUM(PT > 1) & (1 < ANUM(('pi+' == ABSID) & (MIP PCHI2DV (PRIMARY) > 5))) "
Makerau.Mothercut = " (M > 400. MeV) & (M < 2060. MeV)
& (BPVDIRA > 0.99) & (VFASPF(VCHI2) < 25 )"
```

4 MVA

4.1 Goal

The objective of the Multivariate Analysis (MVA) stage is two-fold(8; 12):

1. Estimate the appropriate BDT cut to achieve a signal-to-background (sig/bkg) ratio of approximately 0.10, a requirement for the subsequent MF to measure the branch fraction.

2. Estimate the integrated luminosity required to observe the $D_s^+ \to \tau^+\nu_\tau$ decay in the SMOG experiment with a significance of '5σ' and compare it to the integrated luminosity of SMOG data collected in 2017.

It is crucial to avoid confusing these two distinct goals:

The first goal involves determining the BDT cut that will effectively suppress the background and achieve a sig/bkg ratio high enough to enable accurate branch fraction calculation.

The second goal pertains to finding the minimum amount of data needed to statistically detect a signal from the background with a significance of 5 standard deviations after applying the BDT cut.

To achieve these objectives, a carefully selected set of collected variables is used.

4.2 Collected Variables

Given that the estimated signal-to-background (sig/bkg) ratio is 2.17×10^{-2}, significantly smaller than 0.10, it is essential to select a set of variables with weak correlation and high discriminating power.

The final set of variables selected for the multivariate analysis (MVA) is listed in the last row of Table 3. The differences in shape between the signal and background are illustrated in Fig 5. These variables are categorized into two types: "Original Variables" and "Derived Variables."

Table 3: Collected variables for the multivariate analysis.

Original Variables			Derived Variables	
Mass	Kinetic	Isolation	Angle	Kinetic
tau_M	max_pip_pim_M	tau_EW_0.50_nc_mult	Theta	TaupR_1
max_pip_pim_M	tau_PT	tau_EW_0.00_nc_sPT	TauAngle	Tautr
min_pip_pim_M	tau_P	tau_0.50_cc_mult	pim_pip_theta	
	TauFlightDistance	tau_0.50_cc_sPT	pim_theta	
	tau_FDCHI2_OWNPV	pim_ConeIso		
	tau_IPCHI2_OWNPV	pip2_IsoSumBDT		

4.2.1 Original Variables

The "Original Variables" include mass variables, kinetic variables, and isolation variables related to the pions used in the reconstruction process. Specifically:

- The mass variables τ_M, *max_pip_pim_M*, and *min_pip_pim_M* correspond to the invariant mass of 3π, the maximum $\pi^+\pi^-$ invariant mass, and the minimum $\pi^+\pi^-$ invariant mass, respectively.

- The kinetic variables tau_*PT*, tau_*P*, TauFlightDistance, tau_FDCHI2_OWNPV, and tau_IPCHI2_OWNPV pertain to the transverse momentum (PT) and momentum (P) of 3π, the tau flight distance (FD), and the impact parameter (IP) at the tau decay point.

- Isolation variables are denoted as tau_ ∗ _ ∗ _∗. Here, the first asterisk corresponds to the cone's angle, the second refers to the charge of the particles counted within the cone (nc or cc), and the third relates either to the number of particles (mult) or to their momentum (PZ, sPT, maxPt_PT).
- A selection process was performed to choose variables with weak inter-correlation. Within each nc and cc, momentum-related variables showed strong correlation. Therefore, only the top-ranking four variables of forms ∗_nc_mult, ∗_nc_P, ∗_cc_mult, and ∗_cc_P were adopted to minimize redundancy.
- Similarly, to avoid strong correlations, only one variable was selected from each category of ∗_ConeIso and ∗_IsoSumBDT.

4.2.2 Derived Variables

The "Derived Variables" category includes angle variables and kinetic variables that pertain to both the pions used in the reconstruction process and the τ candidates requiring additional calculations. Detailed calculations for these variables are provided in Appendix A. The angle variables are:

- **Theta**: The angle between the momentum vector of 3π ($\vec{p}_{3\pi}$) and the z-axis in the laboratory frame.
- **TauAngle**: The angle between the momentum vector of the τ candidate ($\vec{p}_{\tau}$) and the z-axis in the laboratory frame.
- **pim_pip_theta**: The angle between the momentum vectors $\vec{p}_{\pi^+}$ and $\vec{p}_{\pi^-}$ in the rest frame of 3π.
- **pim_theta**: The angle between the momentum vector $\vec{p}_{\pi^-}$ and the laboratory momentum vector of 3π ($\vec{p}_{3\pi.lab}$) in the 3π rest frame.

Additionally, the derived kinetic variables related to the τ candidate are:

- **TaupR_1**: Represents the retrieved momentum of the τ candidate.
- **Tautr**: Denotes the lifetime of the τ candidate in its rest frame.

Among the derived variables, the angle variables are relatively powerful due to its high rank, as listed in Table 4

These top-ranked angle variables exhibited promising potential for enhancing the separation between signal and background events. Notably, the reason for their importance is evident from their high ranks among the total of 20 derived variables.

The correlations among the finally collected variables are depicted in Fig. 2, and the ranking of angle variables is provided in Table **??**. As shown in Fig. 2, the correlations among the finally collected variables are visualized. These variables exhibit weak correlations with one another, which is advantageous for the multivariate analysis.

4.3 Results

In line with the objectives set in the MVA stage, we present our findings that address the two-fold goals:

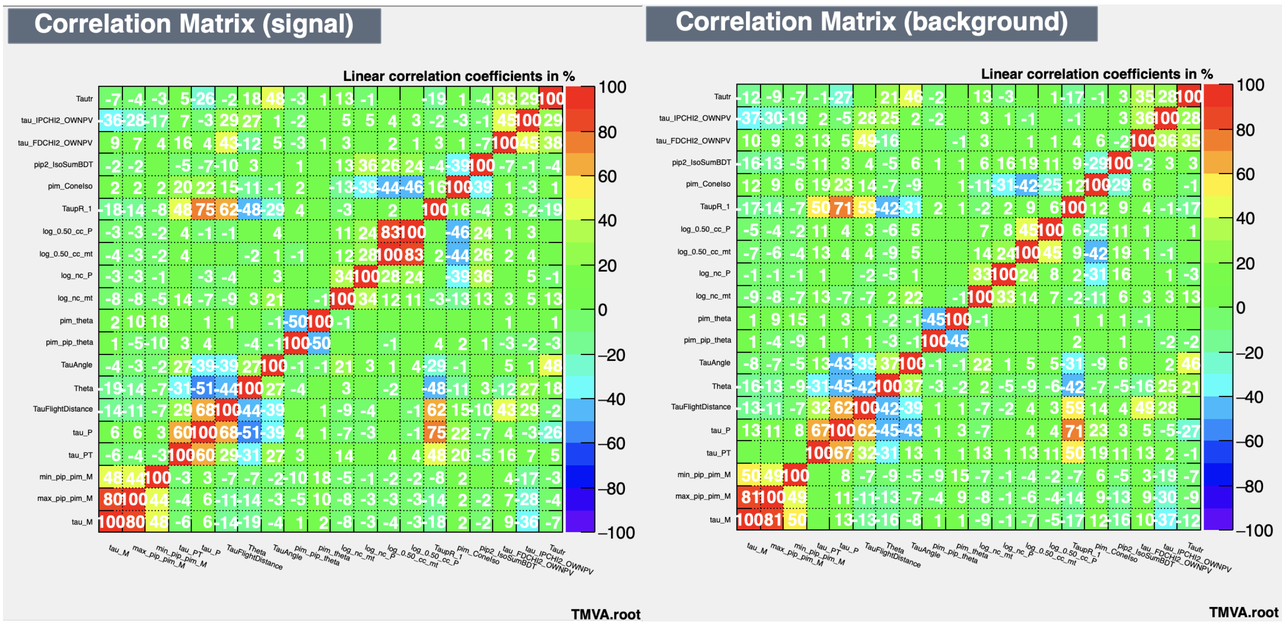

Figure 2: Correlations among the finally collected variables.

Table 4: Rank of some angle variables

Rank	Variables
7	pim_theta
9	pim_pip_theta
10	TauAngle

4.3.1 Achieving the Desired Signal-to-Background Ratio

As per our first goal, we aimed to determine the BDT cut that would effectively suppress the background and achieve a sig/bkg ratio conducive for accurate branch fraction calculation.

- When combining the data, the signal data must be matched with the background data based on the Branching Fraction. Consequently, 553 signal events and 25,454 background events were considered. Our analysis yielded an estimated sig/bkg ratio of 2.17×10^{-2}.
- Using this estimated sig/bkg ratio, we can determine the necessary BDT cut to achieve a target ratio of 0.10.
- Importantly, this sig/bkg ratio remains consistent regardless of data quantity. Similarly, the BDT cut required to achieve a 0.10 ratio is also independent of data size, ensuring its applicability across datasets of varying magnitudes.
- Detailed specifications of the BDT cut and the resulting sig/bkg ratio are presented in Table 5.

4.3.2 Estimating the Required Integrated Luminosity

Our second goal was to determine the minimum amount of data (integrated luminosity) necessary to statistically distinguish a signal from the background with a significance of 5

Table 5: Estimated values for MVA results. The BDT cut is required to achieve a sig/bkg ratio larger than 0.10.

BDT cut	Integrated luminosity
BDT $> 5.65 \times 10^{-2}$	6.74pb^{-1}

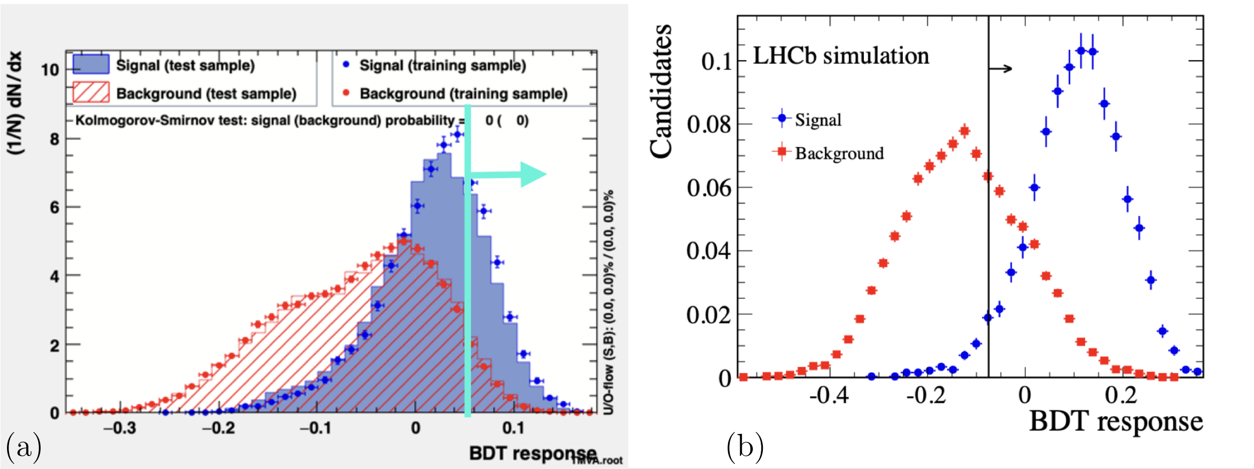

Figure 3: Plots for BDT cutting used in (a) our case and (b) other papers(8; 12).

standard deviations after applying the BDT cut.

- With a significance of 3.44 standard deviations (σ), our current data size is insufficient to calculate the Branching Fraction. To achieve 5σ significance, the estimated minimum integrated luminosity required is 6.74 pb^{-1}.

- To further elaborate, we had a signal of 132 events and a background of 1302 events after applying the BDT cut. The significance $S/\sqrt{S+B}$ is calculated to be 3.44, which is less than the desired 5. Using the approximation $S/\sqrt{S+B} \sim \sqrt{N}$, we estimated that a combined signal and background sample larger than 3023 events after the BDT cut is required to achieve a 5σ significance.

- For the D^0 background, out of the total 3023 events, 1175 events are due to $D^0 \to 3\pi X$. After applying all relevant cuts, only 1067 events survive out of the initial $N_{mc} = 5343095$ events. The integrated luminosity required for the calculation is determined as $L = \frac{N_{\text{required}}}{\sigma B \epsilon_g \epsilon_c} = 6.74\,\text{pb}^{-1}$ using the D^0 channel.

- To avoid confusion, it's worth noting that considering only a single channel is sufficient. Information on other decays, such as Fraction Function and branching fractions shown in Table 2, has already been considered when the total sample is combined.

- The estimated integrated luminosity required to observe the signal with a ' 5σ ' significance is $6.74\,\text{pb}^{-1}$. This value is larger than the 2017 SMOG integrated luminosity of $200\,\text{nb}^{-1}$(14; 15). This comparison underscores that we currently lack the necessary data to extract our desired decay from the background. Therefore, in order to achieve the goal of observing the $D_s^+ \to \tau^+ \nu_\tau$ decay, further data collection and analysis are essential.

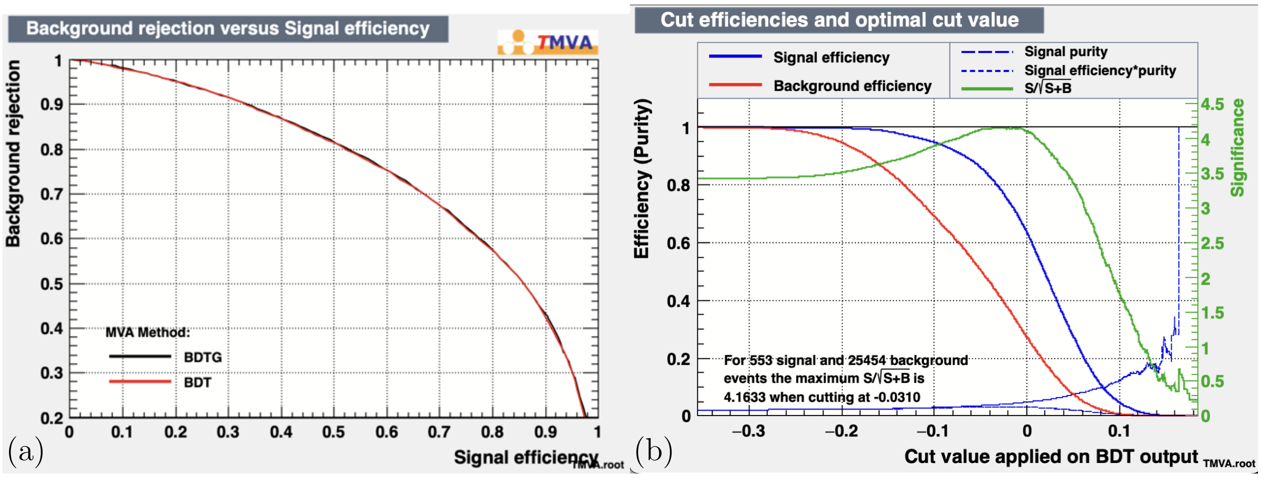

Figure 4: Plots for (a) Background rejection vs Signal efficiency and (b) Cut efficiencies for BDT.

- The list of quantities used to calculate the integrated luminosity is provided in Table 6.

Table 6: Quantities used to calculate the integrated luminosity(9; 10; 11; 13).

σ_{D^0}	$B\,(D^0 \to 3\pi X)$	N_{required}	ϵ_g	$\epsilon_c = \frac{N_{\text{filtered}}}{N_{mc}}$
48.2 μb/nucleon	0.161	1175	0.1854	1.997×10^{-4}

5 Ideas for future improvements

5.1 Multivariable Fitting

As previously mentioned, the size of our dataset is insufficient for multivariable fitting, which aims to determine the branch fraction of the signal using known branch fractions of the background. The error in the branch fraction we obtain is greatly influenced by statistical error. Hence, in our situation, a larger dataset is essential to achieve results within a meaningful and appropriate range. Due to these limitations, we did not proceed with the fitting. Instead, we have suggested variables for potential fitting and identified challenges that may arise during the fitting process.

5.2 Collected Variables

We implemented a more extreme cutting (as shown in Fig 3.a) compared to the BDT cutting used in other papers (as seen in Fig 3.b). Consequently, in our case, it is difficult to use mva_BDT, tau_M, and tautr, which are commonly used variables when conducting MF in other papers.

As a result of extreme BDT cutting, the difference in shapes became hard to discern as shown in Fig 5. Therefore, we selected the top 6 variables for MF as listed in Table.7 using the ranking results from MVA.

Since we did not have enough MC samples, MF has not performed yet.

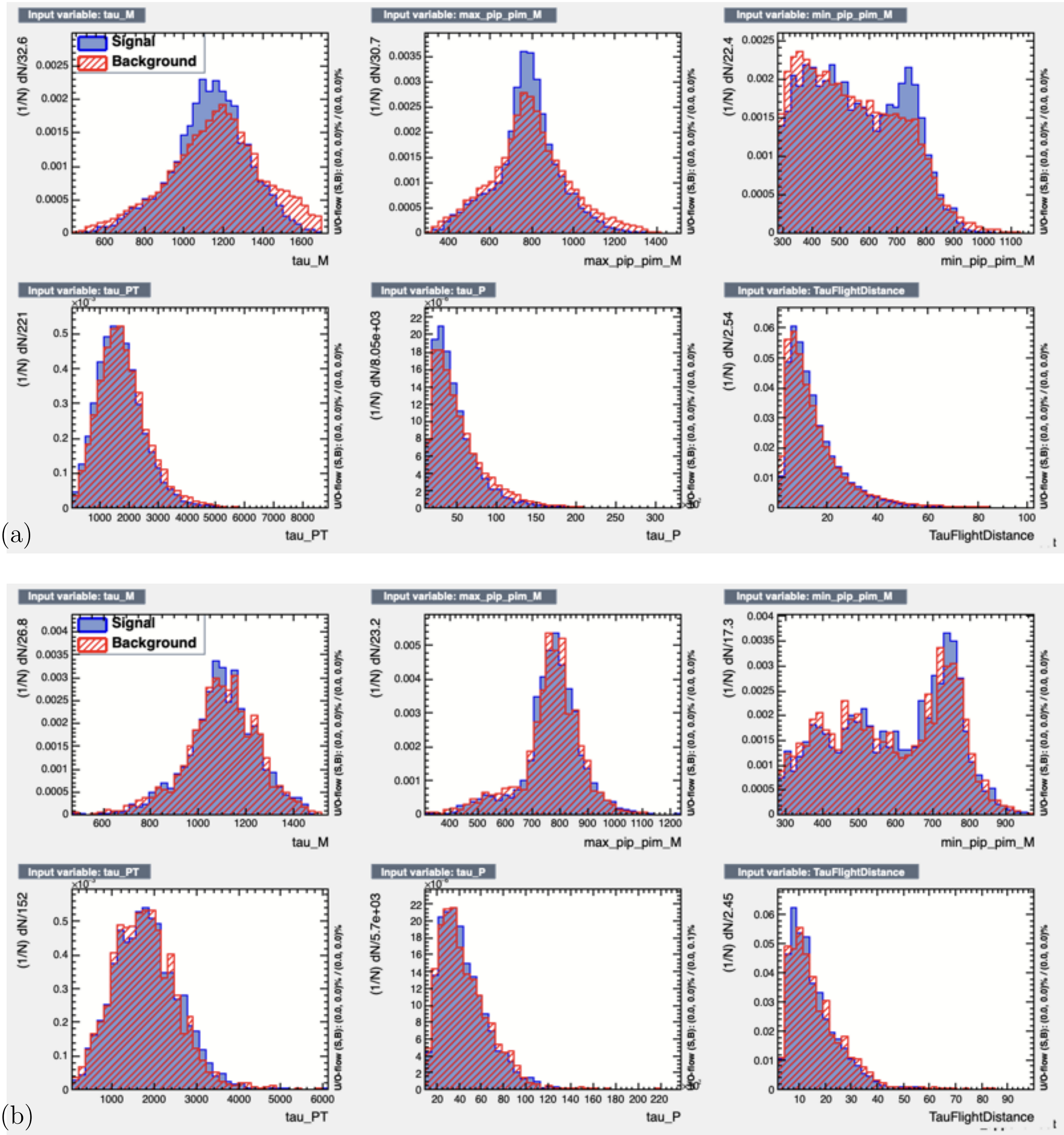

Figure 5: Plots for variables (a) before cutting and (b) after cutting. In the plots of each variable, it is evident that the distinctive differences in distribution shapes between the signal and background samples significantly diminish after the application of cutting.

5.3 Need for Bent Crystal Methodology

For the reason we performed extreme BDT cutting, it's natural that only the background samples similar to signal remain as shown in Fig 5. As a result, the difference in distributions between signal and background for each variable decreases. Thus, we need other ways to suppress the charm background : 'Bent Crystals"

There are three reasons why taking advantage of bent crystals is useful(4; 16):

1. **Suppression of Charm Background:** Only a fraction of τ originating from $D_s^+ \to \tau\nu$

Table 7: Variables for MF with ranks. This MVA analysis was performed after BDT cutting. As a result, its findings differ from the MVA analysis conducted on data prior to the BDT cutting.

Rank	1	2	3	4	5	6
Variables	mva_BDT	pip2_IsoSumBDT	min_pip_pim_M	TauFlightDistance	pim_theta	max_pip_pim_M

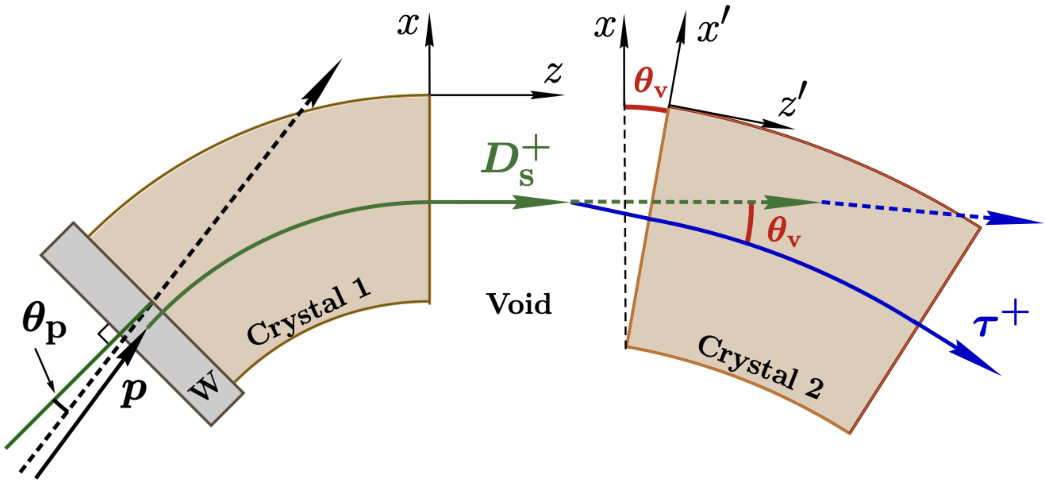

Figure 6: Schematic diagram of the process involving two bent crystals selecting τ from D_s^+ and suppressing other backgrounds(16)

decay can pass through the second crystal, as illustrated in Fig 6. Consequently, the charm background is effectively suppressed. As a result, the need for extreme Boosted Decision Tree (BDT) cutting is eliminated, ensuring that the discriminatory power of the variables remains high. Considering that the branch fraction is obtained by facilitating the Multivariate Analysis (MVA) to the variables, the error in the branch fraction determined by the MVA would notably decrease.

2. **Additional Variables for MVA and MF:** Bent crystals also provide other valuable variables for both the MVA and the Matrix Formalism (MF), such as θ_v which is related to the mean value of the angle between the direction of the incoming D_s^+ and the outcoming τ.

3. **Evaluation of Meaningful Values:** Furthermore, it becomes possible to evaluate other meaningful quantities, such as Electric Dipole Moment (EDM) and Magnetic Dipole Moment (MDM), by quantifying the extent to which the spin of τ rotates.

6 Conclusion

6.1 Summary

- We have conducted a feasibility study on detecting $D_s^+ \to \tau^+ + \nu_\tau$ with $\tau^+ \to 3\pi X$ in SMOG collisions.

- Our primary objective was to suppress the substantial charm background.
- Multivariate Analysis (MVA) was employed to suppress the background.
- To achieve a signal-to-background ratio of approximately 0.1 for a possible fit, the BDT cut is $BDT > 5.65 \times 10^{-2}$.
- To achieve 5σ observation of $D_s^+ \to \tau^+ + \nu_\tau$ in the SMOG configuration, the estimated integrated luminosity is $6.74\,\mathrm{pb}^{-1}$.
- To perform a multivariable fit (MF), the set of collected variables is 'mva_BDT, pip2_IsoSumBDT, min_pip_pim_M, TauFlightDistance, pim_theta, and max_pip_pim_M', as listed in Table.7.

6.2 Further Research

- Generate a sufficient quantity of Monte Carlo (MC) samples to enable a multivariable fit. Additionally, perform a multivariable fit to reevaluate $B(D_s^+ \to \tau^+ + \nu_\tau)$ and estimate the ranges of both statistical and systematic errors.
- Conduct a feasibility study using the employed bent crystal configuration. Building upon the understanding of SMOG, it is possible to engage in simulations and investigations regarding the practical utilization of bent crystals. This involves capitalizing on their strengths, which include suppressing the significant charm background, introducing new high-discriminating power variables, and enabling measurements of the Electric Dipole Moment (EDM) and Magnetic Dipole Moment (MDM) of τ which are relate to probing the need for New Physics.

Acknowledgements

I owe a great deal of gratitude to several individuals without whom this project would not have been possible::

- To **Jinlin**, whose paper on bent crystals laid the groundwork for my project. I am deeply appreciative of the guidance and oversight provided throughout.
- My sincere thanks go to **Chen**, who generously devoted his time every time I had questions regarding programming and the overall research methodology, answering with clarity and patience.
- I extend my gratitude to **Mengzhen**, whose sharp and consistent logical insights were invaluable. His sense of humor and kindness greatly assisted in my acclimatization at CERN.
- I would also like to thank **Nicola** and **Andrea**, the experts on SMOG, whose assistance was paramount to this research.

Appendices

A Derivation of kinetic variables

For the reason the information of neutrinos in τ^- cannot be acquired, it is impossible to fully reconstruct the information of τ candidates. However, we can obtain estimated values of them by this assumption: The distance between the PV and the generated point of τ is small. Adopting this assumption, we can get the estimated flight direction of τ by subtracting the position vector of the reconstructed decay point of 3π from that of PV.

We can readily obtain the flight distance, standardized deviation, CHI square of the flight distance, and impact parameter of τ. Each variable is named 'TauFlightDistance', 'TauSTdDev_Z', 'tau_FDCHI2_OWNPV', and 'tau_IPCHI2_OWNPV' respectively.

A.1 Momentum of τ

According to the energy-momentum conservation, we can retrieve the 4-momentum of τ with the flight direction. The magnitude of the momentum is given by:

$$p = \frac{p_3\alpha \pm E\sqrt{\alpha^2 - 4M_\tau^2(E^2 - p_3^2)}}{2(E^2 - p_3^2)} \tag{3}$$

where $\alpha = M_\tau^2 + M_{3\pi}^2 - M_\nu^2$. Here, E represents the energy of 3π, and p_3 denotes the component of the 3π momentum that is parallel to the direction of τ.

A.2 Sign Determination

The sign in the numerator in Eq. 3 can be either plus or minus, with equivalent validity. In the tau-rest frame, those two types of cases will be equally possible for the given $p_{3\pi}$. The red and blue ones give the $-$ and $+$ sign respectively.

We confirmed that both signs are equally possible by simulation. Eq. 3 can be formulated as follows 4:

$$(p - p_3\alpha)(2(E^2 - p_3^2)) = \pm E\sqrt{\alpha^2 - 4M_\tau^2(E^2 - p_3^2)} \tag{4}$$

We assigned the sign in Eq. 3 such that the sign of the RHS in Eq. 4 matches the sign of the calculated value on its LHS. As shown in Fig. **??**, the difference between the momentum derived from Eq. 3 and given by simulation is completely 0. Therefore, both signs are equally possible.

A.3 Lifetime of τ

Using the momentum, we can evaluate the lifetime of τ in its rest frame as in Eq. 5.

$$t_\tau = \frac{L}{\gamma v} = \frac{M_\tau L}{\gamma M_\tau v} = \frac{M_\tau L}{p} \tag{5}$$

Here, L represents the flight distance of τ, and p denotes the retrieved momentum derived by Eq. 3.

A.4 Application to other decays

Eq. 3 can be generalized as:

$$p = \frac{p_3 \alpha \pm E\sqrt{\alpha^2 - 4M_1^2\left(E^2 - p_3^2\right)}}{2\left(E^2 - p_3^2\right)} \tag{6}$$

Where, $\alpha = M_1^2 + M_{3\pi}^2 - M_2^2$. These decays are possible in the background:

1. $D^0 \to 3\pi K$: $M_1 = 1865$, $M_2 = 498$
2. $D^+ \to 3\pi\pi^+$: $M_1 = 1870$, $M_2 = 140$
3. $D_s^+ \to 3\pi\pi^+$: $M_1 = 1968$, $M_2 = 140$

Each mass value is from "PDG", expressed in MeV.

A.5 New Variables TaupR$_*$

- TaupR$_*$ means that the sign is randomly assigned.
- $*$ can be $1, 2, 3, 4$.
- Each number means the corresponding process:
  1. $\tau \to 3\pi\nu_\tau$
  2. $D^0 \to 3\pi K$
  3. $D^+ \to 3\pi\pi^+$
  4. $D_s^+ \to 3\pi\pi^+$
- After many iterations, TaupR$_1$ is selected for its high discriminating power.
- Tautr is readily calculated as Eq. 5 from TauFlightDistance and TaupR$_1$.

A.6 Energy of Neutrino in the τ-rest Frame

The energy of the neutrino in the τ-rest frame can be expressed as:

$$\epsilon = \frac{M_\tau^2 + M_\nu^2 - M_{3\pi}^2}{2M_\tau} = \epsilon\left(M_{3\pi}\right) \tag{7}$$

Since this variable is entirely determined by $m(3\pi)$, there is no use in considering this variable.

The $P_\perp$ shown in the figure represents a quantifiable value. It is defined as the component of the neutrino's momentum that is perpendicular to the direction of τ. Notably, this value remains invariant when boosted along the direction of τ. As a result, $P_\perp$ is consistent in both the Lab frame and the tau-rest frame. Given this, there are two potential momentum values of τ that can be determined from the retrieved 3π system.

B Selection of Isolation Variables

B.1 Criteria for Selection

- Only the isolation variables such as “tau_* _” are considered.
- **Aim:**
  - Check the correlation among the isolation variables.
  - Reduce the number of isolation variables put into MVA processes, according to the rank.

The variables named “sPt”, “PZ”, and “maxPt” (referred to as “P variables”) exhibit a strong correlation with each other for each nc and cc. Therefore, we select a total of 4 variables: mult and a P variable, for each nc and cc.

B.2 Correlations

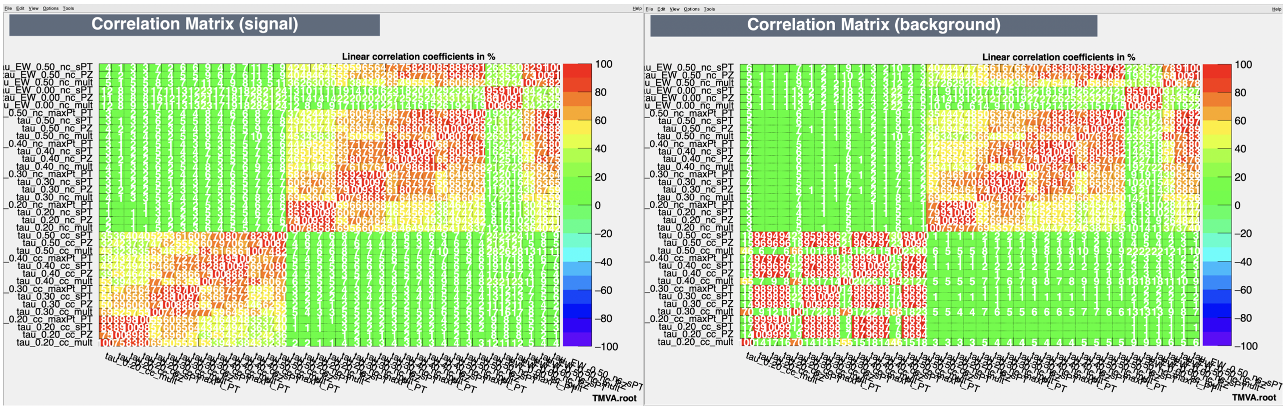

B.3 Variable Rankings

Rank	BDT	BDTG	MLP	BDTB
1	tau_EW_0.00_nc_sPT	tau_EW_0.00_nc_sPT	tau_0.50_cc_mult	tau_0.50_cc_sPT
2	tau_EW_0.00_nc_mult	tau_EW_0.00_nc_mult	tau_0.30_cc_PZ	tau_0.50_cc_mult
3	tau_EW_0.00_nc_PZ	tau_EW_0.00_nc_PZ	tau_0.30_cc_maxPt_P	Tau_0.50_cc_PZ
4	tau_0.50_cc_sPT	tau_EW_0.50_nc_mult	tau_0.40_cc_sPT	tau_0.40_cc_mult
5	tau_0.50_cc_mult	tau_0.50_cc_mult	tau_0.20_cc_PZ	tau_EW_0.00_nc_PZ
6	tau_0.40_cc_maxPt_P	tau_0.50_cc_sPT	tau_0.40_cc_PZ	tau_EW_0.50_nc_mult
7	tau_EW_0.50_nc_mult	tau_EW_0.50_nc_sPT	tau_0.30_nc_sPT	tau_0.40_cc_sPT
8	tau_EW_0.50_nc_sPT	tau_EW_0.50_nc_PZ	tau_0.40_cc_maxPt_P	tau_0.40_cc_PZ
9	tau_EW_0.50_nc_PZ	tau_0.40_cc_maxPt_P	tau_0.30_cc_sPT	tau_0.40_cc_maxPt_PT
10	tau_0.50_cc_PZ	tau_0.50_nc_PZ	tau_EW_0.50_nc_mult	tau_EW_0.00_nc_mult

B.4 Selected Variables

	Mult	P variable
nc	tau_EW_0.50_ nc_mult	tau_EW_0.50_ nc_sPT
cc	tau_0.50_cc_ mult	tau_0.50_cc_ sPT

References

[1] M. Ablikim, M. N. Achasov, et.al, BESIII Collaboration, *Measurement of the branching fraction of leptonic decay $D_s^+ \to \tau^+\nu_\tau$ via $\tau^+ \to \pi^+\pi^0\overline{\nu}_\tau$*, Phys. Rev. D, **104**(3), 032001, 2021. [Online]. Available: `https://link.aps.org/doi/10.1103/PhysRevD.104.032001`

[2] A. Zupanc, I. Adachi, et.al, The BELLE collaboration, *Measurements of branching fractions of leptonic and hadronic D_s^+ meson decays and extraction of the D_s^+ meson decay constant*, Journal of High Energy Physics, **2013**(9), 139, 2013. [Online]. Available: `https://doi.org/10.1007/JHEP09(2013)139`

[3] Particle Data Group, P A Zyla, R M Barnett, et.al, *Review of Particle Physics*, Progress of Theoretical and Experimental Physics, **2020**(8), 083C01, 2020. [Online]. Available: `https://doi.org/10.1093/ptep/ptaa104`

[4] J. Fu, M. A. Giorgi, L. Henry, D. Marangotto, F. Martínez Vidal, A. Merli, N. Neri, J. Ruiz Vidal, *Novel Method for the Direct Measurement of the τ Lepton Dipole Moments*, Phys. Rev. Lett., **123**(1), 011801, 2019. [Online]. Available: `https://link.aps.org/doi/10.1103/PhysRevLett.123.011801`

[5] A. A. Alves Jr. et al., LHCb Collaboration, *The LHCb Detector at the LHC*, JINST, **3**, S08005, 2008. [Online]. Available: `https://doi.org/10.1088/1748-0221/3/08/S08005`

[6] R. Aaij et al., LHCb Collaboration, *LHCb Detector Performance*, Int. J. Mod. Phys. A, **30**(07), 1530022, 2015. [Online]. Available: `https://doi.org/10.1142/S0217751X15300227`

[7] The LHCb Collaboration, *Precision luminosity measurements at LHCb*, Journal of Instrumentation, **9**(12), P12005, 2014. [Online]. Available: `https://doi.org/10.1088/1748-0221/9/12/p12005`

[8] R. Aaij, B. Adeva, M. Adinolfi, et.al, LHCb Collaboration, *Test of lepton flavor universality by the measurement of the $B^0 \to D^{*-}\tau^+\nu_\tau$ branching fraction using three-prong τ decays*, Phys. Rev. D, **97**(7), 072013, 2018. [Online]. Available: `https://link.aps.org/doi/10.1103/PhysRevD.97.072013`

[9] M. Lisovyi, A. Verbytskyi, O. Zenaiev, *Combined analysis of charm-quark fragmentation-fraction measurements*, The European Physical Journal C, **76**(7), 397, 2016. [Online]. Available: `https://doi.org/10.1140/epjc/s10052-016-4246-y`

[10] M. Ablikim, M. N. Achasov, P. Adlarson, et.al, BESIII Collaboration, *Measurement of the absolute branching fraction of the inclusive decay $D_s^+ \to \pi^+\pi^+\pi^- X$*, Phys. Rev. D, **108**(3), 032001, 2023. [Online]. Available: `https://link.aps.org/doi/10.1103/PhysRevD.108.032001`

[11] M. Ablikim, M. N. Achasov, P. Adlarson, et.al, BESIII Collaboration, *Measurements of the branching fractions of the inclusive decays $D^0(D^+) \to \pi^+\pi^+\pi^- X$*, Phys. Rev. D, **107**(3), 032002, 2023. [Online]. Available: `https://link.aps.org/doi/10.1103/PhysRevD.107.032002`

[12] R. Aaij, B. Adeva, et.al, LHCb Collaboration, *Measurement of the Ratio of the $B^0 \to D^{*-}\tau^+\nu_\tau$ and $B^0 \to D^{*-}\mu^+\nu_\mu$ Branching Fractions Using Three-Prong τ-Lepton Decays*, Phys. Rev. Lett., **120**(17), 171802, 2018. [Online]. Available: `https://link.aps.org/doi/10.1103/PhysRevLett.120.171802`

[13] R. Aaij, A. S. W. Abdelmotteleb, C. Abellan Beteta, et.al, *Open charm production and asymmetry in pNe collisions at* $\sqrt{s_{NN}} = 68.5\ GeV$, The European Physical Journal C, **83**(6), 541, 2023. [Online]. Available: https://doi.org/10.1140/epjc/s10052-023-11641-5

[14] LHCb Physics, *Ions Fixed Target at LHCb*, [Online]. Available: https://twiki.cern.ch/twiki/bin/view/LHCbPhysics/IonsFixedTarget

[15] SMOG2 Technical Proposal, [Online]. Available: https://cds.cern.ch/record/2651269/files/SMOG2%20Technical%20Proposal.pdf

[16] A. S. Fomin, A. Yu. Korchin, A. Stocchi, S. Barsuk, P. Robbe, *Feasibility of* τ*lepton electromagnetic dipole moments measurement using bent crystal at the LHC*, Journal of High Energy Physics, **2019**(3), 156, 2019. [Online]. Available: https://doi.org/10.1007/JHEP03(2019)156